AIAA JOURNAL
Vol. 31, No. 10, October 1993

# Numerical Investigation of Oscillatory Instability in Shock-Induced Combustion Around a Blunt Body

Akiko Matsuo* and Toshi Fujiwara†
*Nagoya University, Nagoya 464-01, Japan*

**The basic characteristics of oscillatory instabilities of shock-induced combustion around a spherical projectile flying at hypersonic speed is investigated on the basis of numerical simulation using a two-step chemical reaction model. A series of simulations is conducted to understand the mechanism of these oscillatory instabilities. The oscillatory instabilities are clearly observed when the projectile radius is about 7.5–10 times the induction length. Examination of the computed result shows that the oscillatory instability is created by the wave interaction between the bow shock wave and the stagnation point of the body surface. It is clarified that the oscillatory period is closely related to the balance between a shock stand-off distance and an induction reaction length; i.e., the instabilities are caused not only by the wave interaction between the bow shock and the reaction front but also by the compression wave reflected from the stagnation point of the projectile surface toward the bow shock.**

## Introduction

THE shock-induced combustion around a blunt body has been studied for a long time. Especially during the last few years, many papers have reported on the research for the eventual use of shock-induced combustion for hypersonic air-breathing engines. With the advances in computational fluid dynamics, some of the recent studies[1-3] have employed a numerical approach, where the chemically reacting flowfields were simulated and the results were compared with the previous experiments. However, the accuracy and reliability of the software were their only emphasis, and flow characteristics were not investigated. Besides, the projectile velocity was much higher than the Chapman-Jouguet (C-J) detonation speed of the test gas mixture, and only steady-state solutions with no instability were mainly discussed.

One of the famous phenomena of shock-induced combustion is a periodic instability around a hypersonic flying body. There were many reports about the observation of such periodic instability in physical experiments in the 1970s. Figure 1 has been well known for a long time as the typical case of such a periodic instability. This experiment was done by Lehr[4] in 1971. In this experiment, the projectile body has a 15-mm-diam hemispherical projectile and cylindrical afterbody. The projectile is flying at Mach 5.04, which is nearly equal to the C-J detonation speed of the gas mixture, into the test gas of a stoichiometric hydrogen-air mixture at an initial pressure of 0.421 atm. In Fig. 1, some notable features in the flowfield can be deduced. The first is separation between the bow shock and the reaction front. The second is the corrugated reaction boundary, and the third is the striations in the reaction region, which are connected with the corrugated reaction boundary. The fourth is the existence of many waves between the bow shock wave and the reaction boundary, and they are connected with the corrugated reaction boundary. In this flowfield, high frequency oscillations are observed in front of a spherical projectile, and the frequency of the oscillation was reported to be 1.04 MHz. However, these periodic phenomena appear only under certain conditions. Although these phenomena have interesting features, their mechanism is not well understood.

Presented as Paper 91-1414 at the AIAA 26th Thermophysics Conference, Honolulu, HI, June 24–27, 1991; received Sept. 16, 1991; revision received Sept. 8, 1992; accepted for publication Feb. 5, 1993.


*Graduate Student, Department of Aeronautical Engineering. Member AIAA.

†Professor, Department of Aeronautical Engineering. Member AIAA.

## Previous Works

Basically the periodic instability phenomenon is rare in a detonable gas and the three-dimensional mode appears to be preferred. However, Refs. 5 and 6 discussed the generation mechanism of the cyclic combustion oscillations with one-dimensional longitudinal movement based on physical experiments. In particular, the periodic mechanism was discussed using the history of physical variables on the stagnation streamline where a one-dimensional mode is dominant. Their works give an idea of the cyclic mechanism in longitudinal instability. Figure 2 is an x-t diagram between the bow shock wave and the reaction front on the stagnation streamline to explain the wave interaction model proposed by McVey[5] et al.

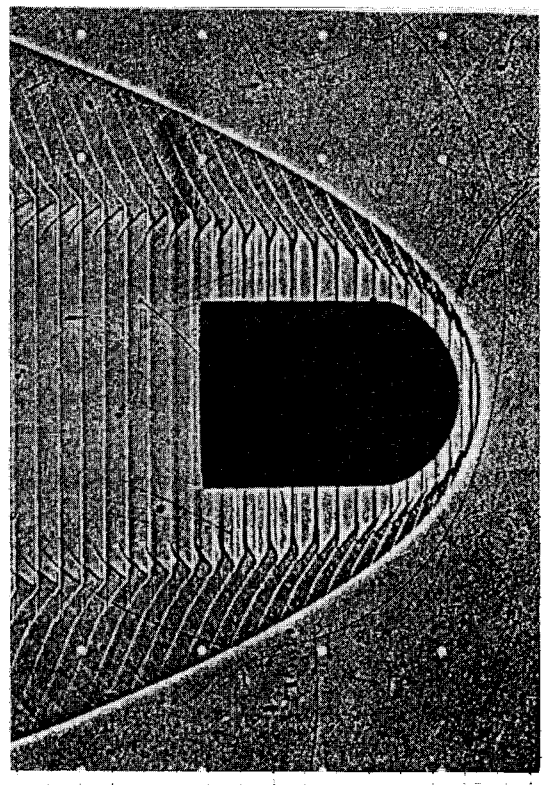

**Fig. 1 Shadowgraph of a spherical nose projectile moving at Mach 5.04 into a premixed stoichiometric hydrogen-air mixture by Lehr (from Ref. 4).**

*Model of Instability Cycle:* In their model (see x-t diagram in Fig. 2), the instability originates in the induction zone that separates the bow shock and the exothermic reaction front in the nose region of the flowfield.

The compression wave is generated at the reaction front and propagates to the bow shock. The contact discontinuity (entropy wave) is created by the interaction of the compression wave with the bow shock. The hot gas after the contact discontinuity begins to react earlier than the gas before the contact discontinuity does. The compression wave is generated as a result of the time-varying reaction rate, depending on the reactant's temperature after the bow shock wave. At a somewhat later time, the contact discontinuity reaches the position of the original reaction front, where there is no more reaction, and a rarefaction wave is generated. The periodic instability comes from the effect on the chemical induction time.

According to this model, the instability wavelength and period only depend on the flow variables behind the bow shock. Suppose this model represents the instability mechanism, the observed phenomena in the experiments should be universal, and this type of oscillatory instability may be observed in the other gas mixture if the gas is under a satisfied condition.

## Numerical Approach

The Zel'dovich-von Neumann-Döring (ZND) wave structure model is useful for understanding the C-J detonation. The ZND model consists of a shock discontinuity followed by a zone of chemical reaction after a certain ignition delay. A simplified model[7,8] to describe the detonation wave, which is based on the ZND wave structure, is used in the present study to analyze shock-induced combustion with the periodic instability. The model consists of a two-step chemical reaction, with the induction and exothermic chemical reaction, instead of all of the elementary chemical reactions occurring behind a leading shock wave. Two reaction progress variables $\alpha$ and $\beta$ are used, and the reacting flowfields around an axisymmetric blunt body is numerically simulated. The specific reaction rate of the induction reaction is given by

$$\omega_\alpha \equiv \frac{\mathrm{d}\alpha}{\mathrm{d}t} = -\frac{1}{\tau_{\mathrm{ind}}} = -K_1\rho \exp\left(-\frac{E_1}{RT}\right) \tag{1}$$

and for the exothermic reaction is given by

$$\omega_\beta \equiv \frac{\mathrm{d}\beta}{\mathrm{d}t} \begin{cases} = 0, & \alpha > 0 \\ = -K_2P^2\left[\beta^2 \exp\left(-\dfrac{E_2}{RT}\right)\right. & \\ \quad \left. -(1-\beta)^2 \exp\left(-\dfrac{E_2+Q}{RT}\right)\right], & \alpha \le 0 \end{cases} \tag{2}$$

The previous model is coupled by the following equations.

$$\frac{\mathrm{D}(\rho\alpha)}{\mathrm{D}t} = \rho\omega_\alpha, \qquad \frac{\mathrm{D}(\rho\beta)}{\mathrm{D}t} = \rho\omega_\beta \tag{3}$$

Here the reaction parameters appearing in Eqs. (1) and (2) are selected as

$$K_1 = 3.0\times 10^{11}\ \mathrm{cm^3/g/s}$$

$$K_2 = 1.875\times 10^{-8}\ \mathrm{cm^4/dyn^2/s}$$

$$E_1/R = 9800\ \mathrm{K}$$

$$E_2/R = 2000\ \mathrm{K}$$

$$Q = 4.0\times 10^{10}\ \mathrm{erg/g}$$

to fit the shock-tube data of $2H_2+O_2+7Ar$ mixture. Here, $K_1$ and $K_2$ are reaction rate constants, and $E_1$ and $E_2$ are activation energies. $Q$ is the exothermic energy per unit gram.

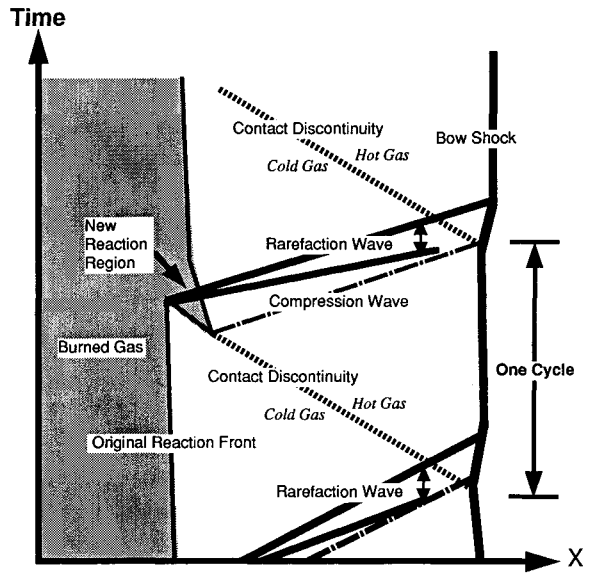


**Fig. 2 x–t diagram on the stagnation streamline proposed by McVey and Toong (from Ref. 5).**

The governing system of equations is written as follows for inviscid flows and axisymmetric geometry under ideal and adiabatic assumptions:

$$\frac{\partial \boldsymbol{Q}}{\partial\tau} + \frac{\partial \boldsymbol{E}}{\partial\xi} + \frac{\partial \boldsymbol{F}}{\partial\eta} + \boldsymbol{H} = \boldsymbol{S} \tag{4}$$

where $\boldsymbol{E}$ and $\boldsymbol{F}$ are the inviscid flux vectors in $\xi$ and $\eta$ directions, respectively; $\boldsymbol{S}$ is the chemical reaction source vector; and $\boldsymbol{H}$ is the axisymmetric source term. The inviscid flux vector and the chemical source vector are

$$\boldsymbol{Q} = J^{-1}\begin{bmatrix}\rho\\ \rho u\\ \rho v\\ e\\ \rho\beta\\ \rho\alpha\end{bmatrix} \qquad \boldsymbol{E} = J^{-1}\begin{bmatrix}\rho U\\ \rho uU+\xi_x P\\ \rho vU+\xi_y P\\ (e+P)U\\ \rho\beta U\\ \rho\alpha U\end{bmatrix}$$

$$\boldsymbol{F} = J^{-1}\begin{bmatrix}\rho V\\ \rho uV+\eta_x P\\ \rho vV+\eta_y P\\ (e+P)V\\ \rho\beta V\\ \rho\alpha V\end{bmatrix}$$

$$\boldsymbol{S} = J^{-1}\begin{bmatrix}0\\0\\0\\0\\ \rho\omega_\beta\\ \rho\omega_\alpha\end{bmatrix} \qquad \boldsymbol{H} = J^{-1}\frac{\rho v}{y}\begin{bmatrix}1\\ u\\ v\\ (e+P)/\rho\\ \beta\\ \alpha\end{bmatrix}$$

Where $P$ and $T$ are the pressure and temperature, respectively, and

$$U = \xi_x u + \xi_y v, \qquad V = \eta_x u + \eta_y v$$

$$P = (\gamma-1)\left[e - \rho\beta Q - 0.5\rho(u^2+v^2)\right] \tag{5}$$

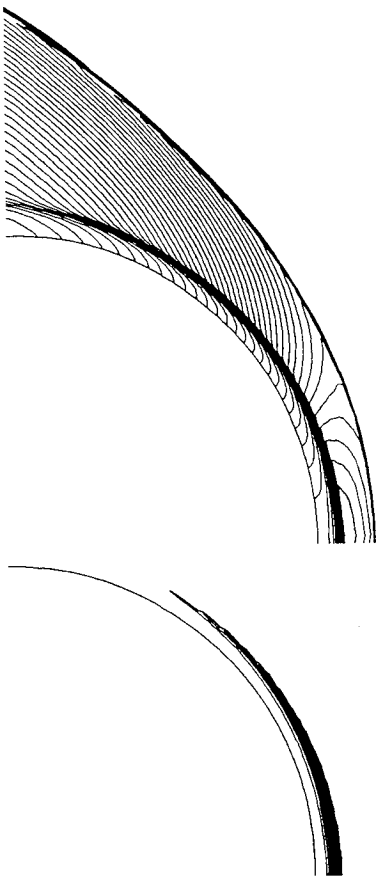


**Fig. 3 Contour plots of projectile radius $5L^*$: a) density and b) $\rho\omega_\beta$.**

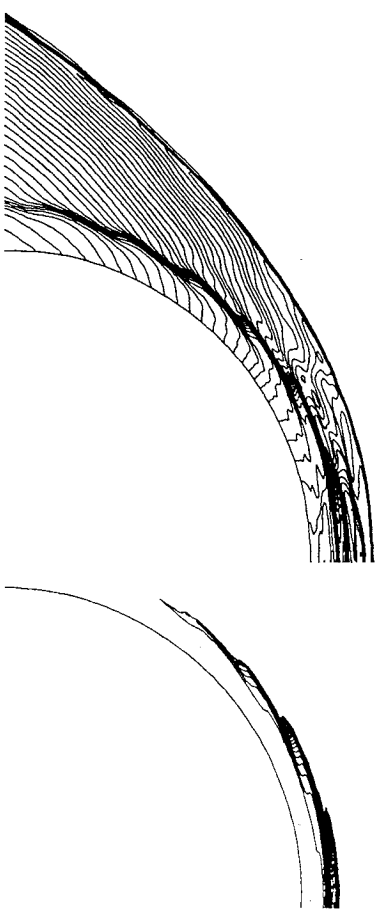


**Fig. 4 Contour plots of projectile radius $7.5L^*$: a) density and b) $\rho\omega_\beta$.**

Our experience indicated that the grid resolution is critically important to describe the wave interaction. The present chemical reaction model does not require excessive computer time and memory, which allows us to use very fine mesh distributions. This is another reason we used this simplified model.

In the present simulation, a TVD formulation[9] with explicit time integration is used. A locally adaptive grid is used to reduce the mesh size behind the bow shock wave and to resolve the wave interactions. The length $L^*$, which is the induction length of the plane C-J detonation corresponding to the incoming gas mixture, is used to nondimensionalize the length scale. The length $L^*$ is 3.654 mm in this case.

## Numerical Results

Ballistic range experiments with the projectile provide us with accurate data of the flowfield, but do not provide the time evolving data on the stagnation streamline to explain the detailed mechanism for instability. The present work investigates the physics of the shock-induced combustion by the numerical simulations, with the focus on the mechanism of the oscillatory instability.

As observed in the physical experiment done by Lehr[4] (see Fig. 1), the reaction boundary is separated from the bow shock wave, and the periodic instability occurs. The $\alpha$–$\beta$ two-step chemical reaction model used in this study does not exactly describe the behavior of each species of the gas mixture. In addition, the treated gas mixture is different from that used by Lehr. However, the basic characteristic of the oscillatory instabilities in the shock-induced combustion is considered to be a more universal phenomenon if the oscillatory mechanism is caused by the wave interaction, which is proposed by McVey and Toong.[5] Thus, verifying and improving the proposed mechanism may be possible by the present simulations, although an $\alpha$–$\beta$ two-step reaction model for the different gas mixture is used.

Throughout our simulations we chose a Mach number of 4.8 as the incoming flow speed, because the C-J detonation Mach number of the present gas mixture is 4.8. It is known that the behavior of shock-induced combustion firing around the C-J velocity is unstable; for example, Lehr's experiment gives 0.99 for the projectile velocity over the C-J value. In our simulations we have two important parameters: one is the spherical projectile radius and the other is the incoming Mach number. A series of simulations was conducted for various projectile radii, and the computed results for three projectile radii, $5L^*$, $7.5L^*$, and $10L^*$, are discussed in the following section.

*Parametric Studies:* To understand the qualitative difference of the flowfield, the density and the $\rho\omega_\beta$ contours are plotted for the three cases. The $\rho\omega_\beta$ is the source term (mass production rate) of Eq. (3) and shows the progress of the exothermic reaction.

1) $5L^*$: Figure 3a shows the density contour plots, and Fig. 3b shows the $\rho\omega_\beta$ of the projectile radius $5L^*$ case. The sudden density change in the region between the bow shock and the body surface indicates the reaction boundary of the burned gas by the exothermic reaction. The $\rho\omega_\beta$ contour plots indicate the region progressing the exothermic reaction. No oscillations are observed along the reaction boundary, and the reaction progresses smoothly. The density residual converges gradually during the computation, and the solution can be understood as the case of a nearly steady-state solution.

2) $7.5L^*$: Figures 4a and 4b are the contour plots of the projectile radius $7.5L^*$ case. The corrugated reaction boundary is observed along the entire projectile body behind the bow shock in the density contours of Fig. 4a. The $\rho\omega_\beta$ contour plots in Fig. 4b correspond to the reaction boundary in Fig. 4a and show that the corrugated reaction-progressing region is restricted only in the region near the axis of the spherical projectile. The phenomenon is almost periodic with high frequency and small amplitude. Since the reaction-progressing region is not seen in the downstream in Fig. 4b, the corrugated reaction boundary moves with the fluid with no reaction progress.

3) $10L^*$: Figures 5a and 5b show the contour plots of the projectile radius $10L^*$ case. The corrugated reaction boundary is observed behind the bow shock, and the phenomenon is periodic, similar to the density contour plots in the case of $7.5L^*$. However, the frequency relative to the projectile radius in the case of $10L^*$ is lower than that in the case of $7.5L^*$. An instability pattern similar to the experiment in Ref. 4 (shown in Fig. 1) appeared in the present numerical simulation. The region of $\rho\omega_\beta$ that corresponds to the corrugated reaction boundary observed in the density contour plots also forms the corrugated pattern, but only in front of the spherical body as is seen in Fig. 5b. The $\rho\omega_\beta$ is not observed downstream of the flowfield. This result indicates that the exothermic chemical reaction terminates and that the reaction boundary moves with the fluid.

The striations in the reaction region seen in Fig. 1 are not observed in either Figs. 4a or 5a, although all the other features are observed. The postprocessor,[10] which simulates the three-dimensional shadowgraph system and generates an output similar to the experiment from the computational result, is used to produce the computational shadowgraph pattern. The result is shown in Fig. 6, where the vertical lines or the striations in the reaction region are now clearly observed. The result suggests that the striations in the reaction region in Fig. 1 are the three-dimensional image of the corrugated reaction boundary.

The relation between the projectile radii and the instabilities were studied. It seems that the instabilities strongly depend on the relation between the shock stand-off distance and the induction length. Compare the induction length on the stagnation streamline in the three previous cases. The geometry of the projectile is the same, but the physical length is different. In a chemically reacting flowfield, two types of length scale exist: the body length and the reaction length. Although the projectile radius changes, the chemical reaction induction length does not change and becomes relatively small compared with the shock stand-off distance. Since the basic length scale is not unique, both length scales are important for the flow features.

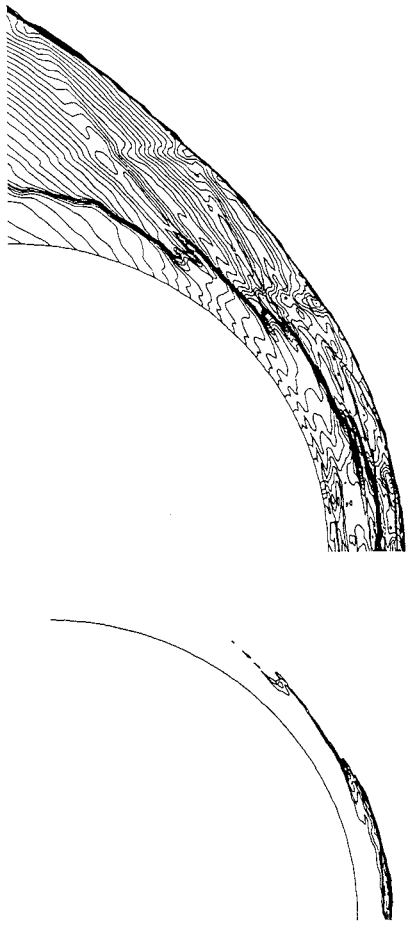


**Fig. 5 Contour plots of projectile radius $10L^*$: a) density and b) $\rho\omega_\beta$.**

## Instability Mechanism

### Time Evolution of Oscillatory Cycle

Figure 7 is the close-up view of the time evolving contour plots of $\rho\omega_\beta$ in the nose region of the spherical projectile showing one cycle from the initiation to the termination of the oscillatory instability in the case of projectile radius $10L^*$. The instability cycle is as follows:

1) At the time 2, a new reaction region is generated in front of the original reaction front around the stagnation streamline.

2) From times 2 to 5, the new reaction region grows up in front of the original reaction front.

3) At the time 6, the original reaction front is coupled with the new reaction region.

4) From times 6 to 9, the corrugated pattern moves along the original reaction front.

5) After the time 10, another cycle begins and the process is repeated.

The corrugated pattern moves with the fluid along the projectile body and disappears further from the projectile, where the exothermic chemical reaction does not occur anymore.

A series of the time evolving contour plots gives us the unstable phenomenon observed in the experiment. Although the oscillatory instabilities are reproduced, the instability mechanism is not well understood in detail only from Fig. 7. To understand the basic phenomenon, the physics on the stagnation streamline is discussed in the next section.

### Wave Interaction

The generation mechanism of the oscillatory instability is discussed using the numerical result of the $10L^*$ projectile radius (Fig. 5). The density history of the physical values (x–t diagram) between the stagnation point of the body surface and

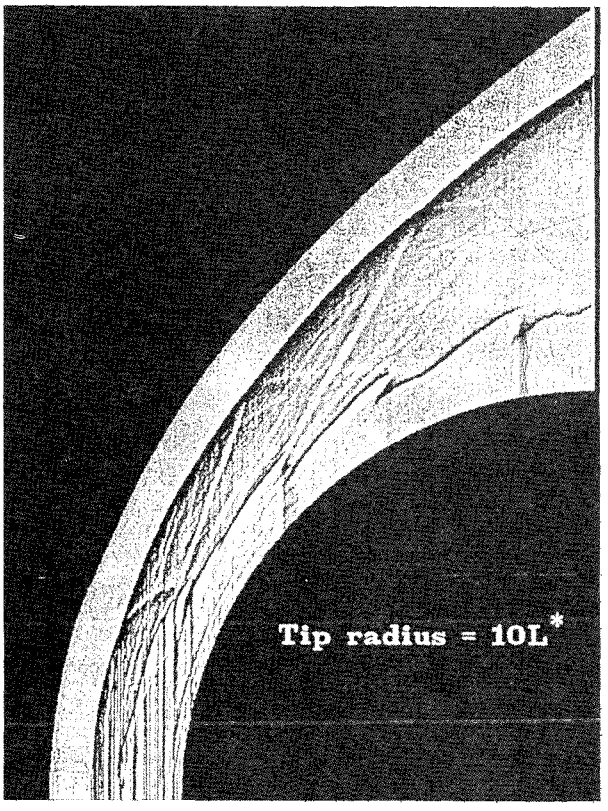


**Fig. 6 Three-dimensional shadowgraph image of projectile radius $10L^*$.[10]**

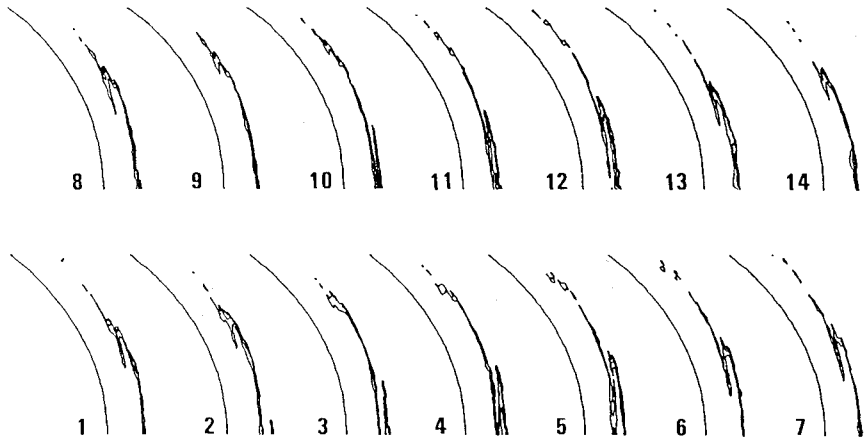


**Fig. 7 Close-up time evolving contour plots of $\rho\omega_\beta$ of projectile radius $10L^*$.**

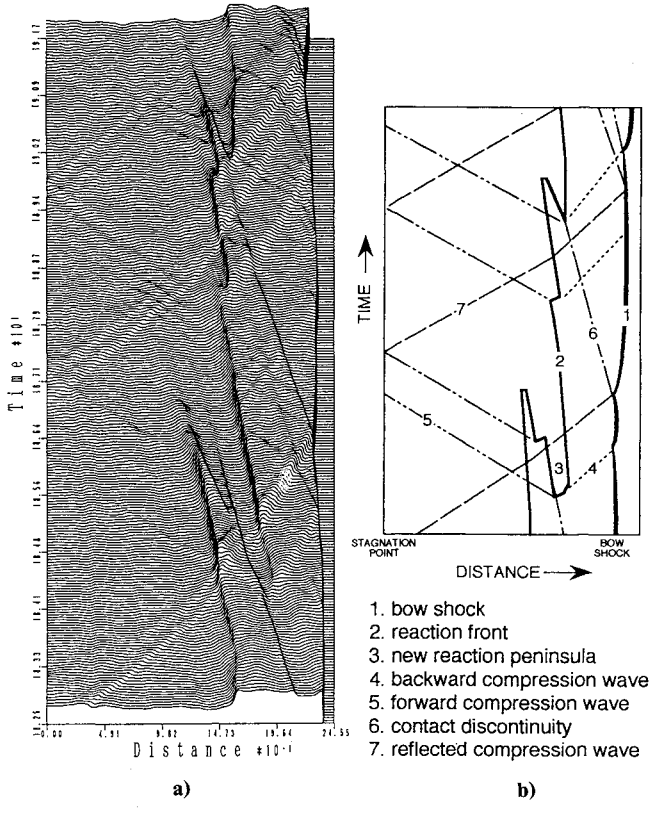


**Fig. 8 Density history (x–t diagram) on the stagnation streamline of $10L^*$ projectile radius: a) level plots and b) schematic representation of density history.**

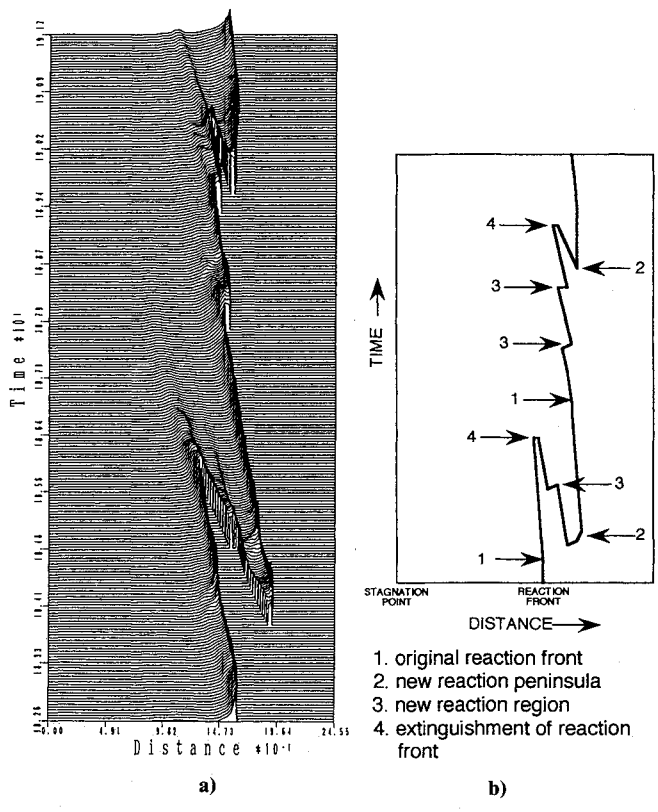


**Fig. 9 $\rho\omega_\beta$ history (x–t diagram) on the stagnation streamline of $10L^*$ projectile radius: a) level plots and b) schematic representation of reaction front.**

the bow shock wave on the stagnation streamline is shown in Figs. 8a and 8b. Figure 8a is the history of density level plots on the stagnation streamline. Each line shows the instantaneous density profile. Figure 8b is the schematic representation of Fig. 8a to help in understanding the wave interactions.

Some remarkable features are observed between the reaction front and the stagnation point in comparison with the x–t diagram shown in Fig. 2. In the wave interaction model in Fig. 2, the waves propagating toward the stagnation point were neglected, and thus only the region between the bow shock wave and the reaction front was discussed. However, our numerical result indicates that the new reaction front generates compression waves not only toward the bow shock wave but also toward the stagnation point. The shock stand-off distance is approximately $0.24\times(\text{radius})=2.4L^*$ in this case. Since the induction length $L^*$ is obtained from the experimental result at the C-J velocity where the steady ZND wave structure model holds, the induction zone must be theoretically $L^*$ on the stagnation streamline behind the normal segment of the bow shock. Therefore, only about 40% of the shock stand-off distance is the induction zone region. The region between the reaction front and the stagnation point is about 60% of the shock stand-off distance and may not be negligible in the wave interaction model. Actually Fig. 8a shows the induction zone whose length is approximately $L^*$. Our mechanism is based on the whole region between the bow shock and the stagnation point on the stagnation streamline. If the induction length is shorter in comparison with the shock stand-off distance, the wave propagating toward the stagnation point may be neglected.

All kinds of waves and changes of physical variables are observed in the density history profile. In Fig. 8a the trace of the bow shock is noticed as a sudden density increase of an incoming uniform flow, and the reaction front is indicated by a sudden density decrease after the bow shock. There are new reaction zones between the original reaction front and the bow shock. Some of them are generated as an isolated area in front of the original reaction surface, connected with the original one and formed as a peninsula. Also, many wave interactions between the bow shock wave and the stagnation point are observed. There are two kinds of cyclic mechanisms. Basically the compression waves are generated at the new reaction front. One wave goes backward (to the bow shock) and the other forward (to the projectile body). The former interacts with the bow shock and generates a contact discontinuity. In general, the temperature on one side of a contact discontinuity is higher than that on the other side. The formation is more like a one-dimensional shock-tube problem. The induction length is highly dependent on the temperature determining the induction time [see Eq. (1)]. The higher temperature fluid has the shorter induction time, since the fluid velocity across the contact discontinuity is basically the same. On the other hand, the latter wave propagates toward the projectile body and reflects on the stagnation point. The reflected wave eventually hits the bow shock and generates a contact discontinuity like the former. These two cyclic wave propagations are basically repeated but do not have an exact periodicity.

### Creation of New Reaction Front

The strength of a compression wave has an important role in determining the position and the strength of a new reaction front. The strength depends on the strength of the explosive reaction. The mass production rate $\rho\omega_\beta$ is useful as a parameter to measure the strength of the reaction and to know where the exothermic reaction progresses. Suppose the mass production per unit time is high. A strong energy release occurs and compression waves are generated. Figure 9a shows the history of the mass-production rate-level plots on the stagnation streamline for the same result as Fig. 8. The schematic representation of Fig. 9a is shown in Fig. 9b to specify the progress along the reaction front. The exothermic reaction progressing region can be recognized in Fig. 9a. The reaction hardly progresses behind the reaction front, which means that the condition reaches chemical equilibrium. Also, there is a notable difference between the original reaction front indicated as (1) in Fig. 9b and the region indicated as (2, 3). Along the original reaction front, the area of high mass production rate is restricted in a very narrow region just after the reaction front. On the other hand, the mass production rate keeps the high level for a certain distance in the peninsula region shown as (2, 3). The length of the high peak is an important factor in determining the strength of the released energy and thus the strength of the compression waves.

The extinguishing of the reaction front specified as (4) in Fig. 9b is observed in Figs. 8 and 9. Reaction progress is observed at (4), but it is not so strong as to generate there.

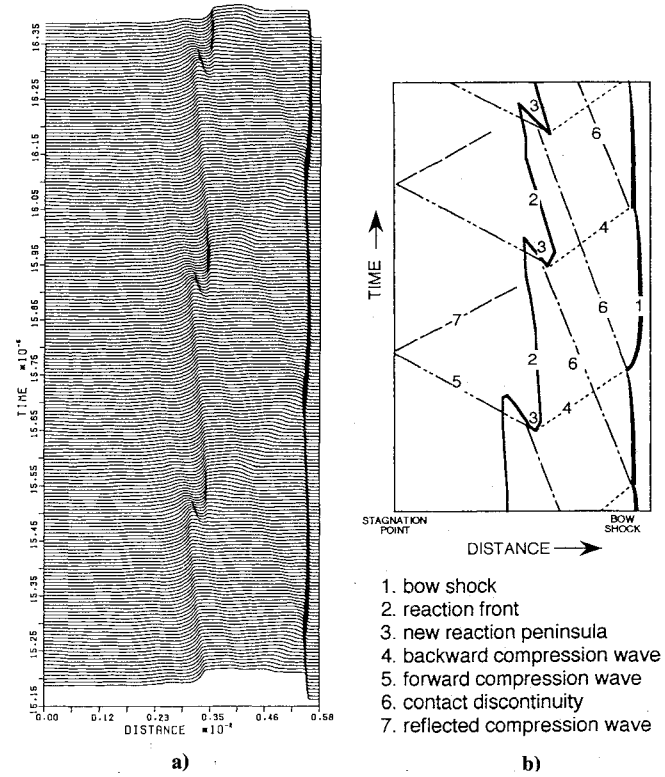


**Fig. 10 Density history (x–t diagram) on the stagnation streamline of $7.5L^*$ projectile radius: a) level plots and b) schematic representation of the density history.**

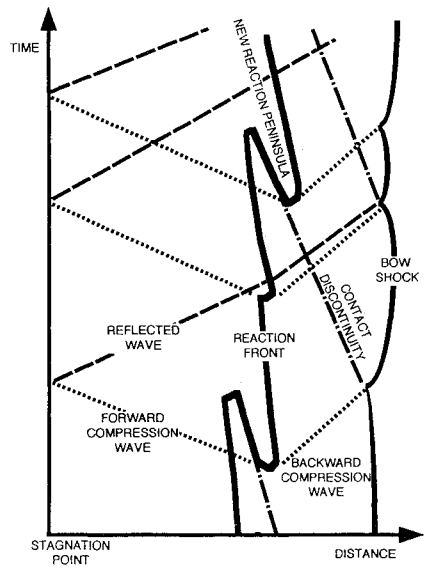


**Fig. 11 x–t diagram of oscillatory mechanism on the stagnation streamline based on the present study.**

### Feature of Oscillation

As observed in Figs. 4a and 5a, the frequency relative to the projectile radius in the case of $7.5L^*$ is higher than that in the case of $10L^*$, even though the induction length relative to the shock stand-off distance is longer in the case of the $7.5L^*$ projectile. As shown in Fig. 10, two oscillatory cycles regularly exist on the stagnation streamline. Since one cycle starts when the other cycle passes the half period, the frequency is doubled. This kind of wave interaction makes the frequency higher, and the transition of the frequency could be observed in the experiments.

## Oscillatory Mechanism Based on the Simulations

Figure 11 is the x–t diagram proposed in the present paper based on our calculations in comparison with Fig. 2. It shows the whole region between the stagnation point and the bow shock on the stagnation streamline. As in the proposed mechanism by McVey and Toong[5] based on the experimental observation, compression waves generated at a new reaction region have an important role for the oscillatory mechanism in this proposed mechanism also. In this proposed mechanism, on the other hand, one of the generated compression waves goes to the stagnation point on the body surface in addition to the compression waves toward the bow shock, finally resulting in a contact discontinuity for the wave interaction with the bow shock wave. The new reaction fronts are formed as a peninsula in the induction reaction region or an additional region of the original reaction front, as seen in Fig. 11.

Although this cyclic mechanism is generated by the compression waves created at the new reaction region, the compression waves are not always effective in making the new reaction, depending on the strength of the compression wave. The basic pattern of the cyclic mechanism repeats itself in Fig. 11, but the features are not exactly the same in detail.

The cyclic mechanism depends on the relation between the shock stand-off distance and induction length, so that a periodic oscillation should be observed when certain conditions are satisfied.

## Conclusions

The basic characteristics of shock-induced combustion around an axisymmetric blunt body have been qualitatively clarified on the basis of numerical simulations. The cyclic mechanism for the generation of oscillatory instability is caused by the wave interactions between the stagnation point and the bow shock wave on the stagnation streamline. The intensive reaction progress accompanied by energy release creates the compression waves that move toward the bow shock. A contact discontinuity is created by the interaction of these compression waves and the bow shock, and a new reaction occurs earlier than the original reaction front due to the higher temperature after the contact discontinuity. The present numerical simulation justified that the model proposed by McVey and Toong can basically explain the oscillatory instabilities observed in shock-induced combustion of previous works.[5,6,11] At the same time, the simulation result suggested the existence of the other cycle orignated by the compression wave toward the projectile body. As a periodic instability pattern is observed in the gas mixture diluted by Argon, and the wave interactions are the key factor for the instability, this periodic instability can occur in other gas mixtures under the satisfied conditions.

Since the previous works are based on experimental results and a simplified one-dimensional wave interaction theory, the exact time evolving data on the stagnation streamline was not available. A numerical approach, on the other hand, supplies it and was confirmed as a useful probing technique for such complex and detailed phenomena.

## References

[1]Lee, S. H., and Deiwert, G. S., "Flux-Vector Splitting Calculation of Nonequilibrium Hydrogen-Air Reactions," *Journal of Spacecraft and Rockets,* Vol. 27, No. 2, 1990, pp. 167–174.

[2]Wilson, G. J., and MacCormack, R. W., "Modeling Supersonic Combustion Using a Fully-Implicit Numerical Method," AIAA Paper 90-2307, July 1990.

[3]Yungster, S., Eberhardt, S., and Bruckner, A. P., "Numerical Simulation of Hypervelocity Projectiles in Detonable Gases," *AIAA Journal,* Vol. 29, No. 2, 1991, pp. 187–199.

[4]Lehr, H. F., "Experiments on Shock-Induced Combustion," *Astronautica Acta,* Vol. 17, Nos. 4 & 5, 1972, pp. 589–597.

[5]McVey, J. B., and Toong, T. Y., "Mechanism of Instabilities of Exothermic Hypersonic Blunt-Body Flow," *Combustion Science and Technology,* Vol. 3, No. 2, 1971, pp. 63–76.

[6]Alpert, R. L., and Toong, T. Y., "Periodicity in Exothermic Hypersonic Flow about Blunt Projectiles," *Astronautica Acta,* Vol. 17, Nos. 4 & 5, 1972, pp. 539–560.

[7]Taki, S., and Fujiwara, T., "Numerical Analysis of Two-Dimensional Nonsteady Detonation," *AIAA Journal,* Vol. 16, No. 1, 1978, pp. 73–77.

[8]Matsuo, A., and Fujiwara, T., "Numerical Simulation of Shock-Induced Combustion Around an Axisymmetric Blunt Body," AIAA Paper 91-1414, June 1991.

[9]Yee, H. C., "Upwind and Symmetric Shock Capturing Schemes," NASA TM-89464, 1987.

[10]Tamura, Y., and Fujii, K., "Visualization for Computational Fluid Dynamics and the Comparison With Experiments," AIAA Paper 90-3031, Aug. 1990.

[11]Buckmaster, J. D. (ed.), "The Mathematics of Combustion," *Frontiers in Applied Mathematics,* Society for Industrial and Applied Mathematics, Philadelphia, PA, pp. 161–164.